



# UNIVERSITÀ DI PARMA

## ARCHIVIO DELLA RICERCA

University of Parma Research Repository

Tuning of a Vertical Spin Valve with a Monolayer of Single Molecule Magnets

This is the peer reviewed version of the following article:

*Original*

Tuning of a Vertical Spin Valve with a Monolayer of Single Molecule Magnets / Cucinotta, Giuseppe; Poggini, Lorenzo; Pedrini, Alessandro; Bertani, Federico; Cristiani, Nicola; Torelli, Martina; Graziosi, Patrizio; Cimatti, Irene; Cortigiani, Brunetto; Otero, Edwige; Ohresser, Philippe; Saintavit, Philippe; Dediu, Alek; Dalcanale, Enrico; Sessoli, Roberta; Mannini, Matteo. - In: ADVANCED FUNCTIONAL MATERIALS. - ISSN 1616-301X. - 27:42(2017), p. 1703600. [10.1002/adfm.201703600]

*Availability:*

This version is available at: 11381/2835296 since: 2024-02-22T15:46:05Z

*Publisher:*

Wiley-VCH Verlag

*Published*

DOI:10.1002/adfm.201703600

*Terms of use:*

Anyone can freely access the full text of works made available as "Open Access". Works made available

*Publisher copyright*

note finali coverpage

(Article begins on next page)

Dear Author,

**Please correct your galley proofs carefully and return them no more than three days after the page proofs have been received.**

If you have not used the PXE system before, please view the Tutorial before checking your proofs:  
[http://wileypxe.aptaracorp.com/pxewileyvch/UserDocument/UserGuide/WileyPXE5\\_AuthorInstructions.pdf](http://wileypxe.aptaracorp.com/pxewileyvch/UserDocument/UserGuide/WileyPXE5_AuthorInstructions.pdf)

Please note any queries that require your attention. These are indicated with red Qs in the pdf or highlighted as yellow queries in the "Edit" window.

Please pay particular close attention to the following, as no further corrections can be made once the article is published online:

- **Names** of all authors present and spelled correctly
- **Titles** of authors are correct (Prof. or Dr. only: please note, Prof. Dr. is not used in the journals)
- **Addresses of all authors and e-mail address of the corresponding author** are correct and up-to-date
- **Funding bodies** have been included and grant numbers are accurate

- The **Title** of the article is OK
- All **figures** are correctly included
- **Equations** are typeset correctly

Note that figure resolution in the PXE system is deliberately lower to reduce loading times. This will be optimized before the article is published online.

**Please send any additional information, such as figures or other display items, to [afm@wiley-vch.de](mailto:afm@wiley-vch.de), and please also indicate this clearly in the PXE "Edit" window by inserting a comment using the query tool.**

**Reprints** may be ordered by filling out the accompanying form.

Return the reprint order form by e-mail with the corrected proofs, to Wiley- VCH: [afm@wiley-vch.de](mailto:afm@wiley-vch.de)

**Please limit corrections to errors already in the text. Costs incurred for any further changes will be charged to the author, unless such changes have been agreed upon by the editor.**

The editors reserve the right to publish your article without your corrections if the proofs do not arrive in time. Note that the author is liable for damages arising from incorrect statements, including misprints.

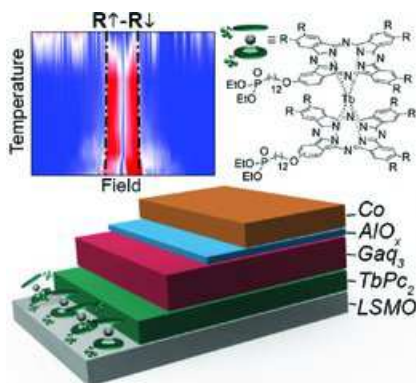


## FULL PAPER

### Molecular Spintronics

G. Cucinotta, L. Poggini, A. Pedrini, F. Bertani, N. Cristiani, M. Torelli, P. Graziosi, I. Cimatti, B. Cortigiani, E. Otero, P. Ohresser, P. Saintavit, A. Dediu, E. Dalcanale, R. Sessoli, M. Mannini\* .....x-xx

#### Tuning of a Vertical Spin Valve with a Monolayer of Single Molecule Magnets



Spinterface tuning of a vertical spin-valve, is achieved by the chemical functionalization of the spin-injecting electrode with a terbium(III) bis(phthalocyaninato) monolayer grafted from solution. Comparing the results obtained with a similar device fabricated including a diamagnetic layer it is possible to evidence that the single molecule magnets film constitutes an additional spin-scattering layer able to control directly the magnetoresistance strength.

# Tuning of a Vertical Spin Valve with a Monolayer of Single Molecule Magnets

Giuseppe Cucinotta, Lorenzo Poggini, Alessandro Pedrini, Federico Bertani, Nicola Cristiani, Martina Torelli, Patrizio Graziosi, Irene Cimatti, Brunetto Cortigiani, Edwige Otero, Philippe Ohresser, Philippe Sainctavit, Alek Dediu, Enrico Dalcanale, Roberta Sessoli, and Matteo Mannini\*

The synthesis and the chemisorption from solution of a terbium bis-phthalocyaninato complex suitable for the functionalization of lanthanum strontium manganite (LSMO) are reported. Two phosphonate groups are introduced in the double decker structure in order to allow the grafting to the ferromagnetic substrate actively used as injection electrode in organic spin valve devices. The covalent bonding of functionalized terbium bis-phthalocyaninato system on LSMO surface preserves its molecular properties at the nanoscale. X-ray photoelectron spectroscopy confirmed the integrity of the molecules on the LSMO surface and a small magnetic hysteresis reminiscent of the typical single molecule magnet behavior of this system is detected on surface by X-ray magnetic circular dichroism experiments. The effect of the hybrid magnetic electrode on spin polarized injection is investigated in vertical organic spin valve devices and compared to the behavior of similar spin valves embedding a single diamagnetic layer of alkyl phosphonate molecules analogously chemisorbed on LSMO. Magnetoresistance experiments have evidenced significant alterations of the magneto-transport by the terbium bis-phthalocyaninato complex characterized by two distinct temperature regimes, below and above 50 K, respectively.

Dr. G. Cucinotta, Dr. L. Poggini,<sup>[+]</sup> N. Cristiani, Dr. I. Cimatti, B. Cortigiani, Prof. R. Sessoli, Dr. M. Mannini  
Department of Chemistry "Ugo Schiff" & INSTM RU  
University of Firenze

Via della Lastruccia 3, 50019, Sesto Fiorentino (FI), Italy

Dr. A. Pedrini, Dr. F. Bertani, N. Cristiani, M. Torelli, Prof. E. Dalcanale  
Dipartimento di Scienze Chimiche  
della Vita e della Sostenibilità Ambientale & INSTM RU  
University of Parma

Parco Area delle Scienze 17/A, 43124, Parma, Italy

Dr. P. Graziosi, Dr. A. Dediu  
Consiglio Nazionale delle Ricerche – Istituto per lo Studio dei Materiali  
Nanostrutturati ISMN-CNR  
Via Piero Gobetti 101, 40129, Bologna, Italy

Dr. E. Otero, Dr. P. Ohresser, Dr. P. Sainctavit  
Synchrotron SOLEIL  
L'Orme des Merisiers Saint Aubin, BP 48, 91192, Gif sur Yvette, France


Dr. P. Sainctavit  
Institut de Mineralogie  
de Physique des Materiaux et de Cosmochimie  
UMR 7590  
CNRS  
UPMC  
IRD

## 1. Introduction

In the last years, the electronic and magnetic structure of interfaces formed between an organic  $\pi$ -conjugated semiconductor and a ferromagnetic layer have been investigated for a large variety of systems.<sup>[1]</sup> The formation of hybrid states with magnetic properties, or specific exchange interactions, has been shown to have a clear impact on spin injection across the interface.<sup>[2]</sup> This topic has a huge interest for both fundamental and applicative research related to organic–inorganic devices like magnetic tunnel junctions, spin valves, memristors, and others, whose performances are strongly affected by the boundary region between the organic and inorganic phases.<sup>[3–9]</sup> Most important achievements have been hitherto obtained by interfac-

MNHN  
4 place Jussieu, F-75252, Paris cedex, France

Correspondence to: Dr. M. Mannini (E-mail: matteo.mannini@unifi.it)

 The ORCID identification number(s) for the author(s) of this article can be found under <http://dx.doi.org/10.1002/adfm.201703600>

[+]<sup>+</sup>Present address: CNRS University of Bordeaux, ICMCB, UPR 9048, F-33600 Pessac, France

DOI: 10.1002/adfm.201703600

ing organic materials with complex ferromagnetic metal oxides, in particular with the lanthanum strontium manganite oxide (LSMO), whose large spin polarization of the surface (nominally 100% at 0 K) and good stability under different conditions may represent a significant advantage with respect to the use of 3D ferromagnetic thin films.<sup>[8]</sup> On the other hand, the use of molecules as building blocks allows to introduce in electronic devices new functionalities due to the almost infinite combination offered by synthesis of complex and tunable molecular objects.<sup>[10]</sup> In particular the introduction of monolayers of magnetic molecules is attracting broad interest thanks to their potential technological applications in molecular spintronics<sup>[11]</sup> and quantum computation.<sup>[12]</sup> Self-assembled monolayer (SAM)-based protocols<sup>[13]</sup> are among the most used techniques to achieve a bidimensional organization of molecules adsorbed on surface. In this context the wet chemistry-based deposition of monolayer of magnetically bistable molecules, known as single molecule magnets (SMM),<sup>[14]</sup> has been widely explored,<sup>[15–21]</sup> evidencing suitable strategies for the stabilization<sup>[19]</sup> or even the enhancement<sup>[21]</sup> of the SMM behavior when these fragile complexes are chemisorbed on surface. We recently adopted a SAM-based strategy to tune the LSMO interface by introducing a monolayer of chemisorbed organic radicals<sup>[22]</sup> that alters the spin injection performances at low temperature through a spin-filtering effect. Here, we aim to combine these concepts by developing a specific functionalization strategy to promote chemisorption of a modified terbium (III) double decker system, an archetypal SMM, on the LSMO surface. A diethyl phosphonate group has been selected as linker agent compatible with the chemistry of the core structure of TbPc<sub>2</sub>. This modified hybrid spin injecting electrode has been then used to realize a vertical organic spin valve comprising Gaq<sub>3</sub> as organic semiconductor and cobalt as the second magnetic electrode. The performances of this type of devices have been compared with those of a similar one obtained by replacing the double decker layer with diamagnetic molecules, the diethyl(11-iodoundecyl)phosphonate, bearing the same linking group promoting the chemisorption. This strategy has been developed in order to disentangle the effect of the chemical functionalization of the manganite, which has been addressed also in earlier reports,<sup>[23,24]</sup> from more specific effects, due to the presence of a layer of magnetic molecules forming an additional spinterface for the spin injection into the organic semiconductor.

## 2. Results

### 2.1. Synthesis and Bulk Characterization of the LSMO-Graftable Tb Double Decker

We synthesized a homoleptic terbium(III) bis-phthalocyaninato (TbPc<sub>2</sub>) complex bearing two peripheral diethyl phosphonate groups (Tb[Pc(PO<sub>3</sub>Et<sub>2</sub>)<sub>2</sub>]<sub>2</sub>, **Figure 1a**) for covalent grafting on LSMO surface. Phosphonic esters ensure the formation of robust monolayers via strong P–O–metal linkages.<sup>[25,26]</sup> Since these anchoring functionalities were found to be unstable under the harsh conditions required for both phthalocyanine (Pc)<sup>[27]</sup> and TbPc<sub>2</sub> formations, the postfunctionalization of already formed TbPc<sub>2</sub> complexes was implemented. The prepara-

tion of the dihydroxy-functionalized double decker Tb[Pc(OH)<sub>2</sub>]<sub>2</sub> was achieved in two steps starting from the asymmetric A<sub>3</sub>B-type phthalocyanine Pc(OPMB), modifying a protocol reported by Pushkarev et al.<sup>[28]</sup> *p*-methoxybenzyl (PMB) group was used as protection of the hydroxyl functionality during the statistical macrocyclization and the subsequent ligand exchange reaction. Instead, the choice of *p*-*tert*-butylphenoxy substituents on Pc's residual positions was required to increase their solubility, hampering the formation of aggregates by steric repulsion. Complex formation was performed reacting the phthalocyaninato ligand Pc(OPMB) with terbium(III) acetyl-acetonate hydrate in 1-hexadecanol at 453 K in presence of lithium methoxide. Tb[Pc(OPMB)]<sub>2</sub> was obtained as a mixture of constitutional isomers in 35% yield and characterized by UV–vis spectroscopy and high-resolution matrix-assisted laser desorption ionization time-of-flight mass spectrometry (MALDI-TOF). The deprotection of the two hydroxyl functionalities with trifluoroacetic acid in DCM at room temperature afforded Tb[Pc(OH)]<sub>2</sub> in quantitative yield. Finally, the introduction of the phosphonate groups was realized via nucleophilic substitution of diethyl 12-bromododecyl-phosphonate (BDP), obtained by microwave assisted Arbuzov reaction between 1,12-dibromododecane and a substoichiometric amount of triethyl phosphite. As demonstrated in our recent works,<sup>[21,29,30]</sup> long aliphatic spacers are required to preserve the reactivity of the peripheral functionalities in the following steps. Tb[Pc(OH)]<sub>2</sub> was reacted with BDP in *N,N*-dimethylformamide (DMF) at 363 K in presence of potassium carbonate. Tb[Pc(PO<sub>3</sub>Et<sub>2</sub>)<sub>2</sub>]<sub>2</sub> was obtained in 48% yield after column chromatography and was characterized by NMR and UV–vis spectroscopies (see Figures S1–S3 in the Supporting Information) and MALDI-TOF. In particular, the MALDI-TOF spectrum (**Figure 1b**) reveals the presence of the molecular peak, with an isotopic distribution pattern in agreement with the theoretical one.

The characterization carried out with traditional DC and AC magnetometry allows a complete evaluation of the magnetic properties of the complex in its bulk phase. As already observed for other TbPc<sub>2</sub> complexes<sup>[31–35]</sup> the hysteresis in the magnetization curves is visible below 15 K thus indicating that the functionalization does not alter significantly the SMM behavior of this double decker system (**Figure 1c**). Zero static field AC susceptibility measurements as a function of temperature are shown in **Figure S4** in the Supporting Information and in the out-of-phase component a frequency dependent peak occurring at relatively high temperatures is visible. The extended Debye model,<sup>[14]</sup> adopted to analyze these data in the range 0.5 Hz–10 kHz, allows to extract the relaxation time,  $\tau$ , of this system for different temperatures (**Figure 1d**). In the high temperature regime,  $T > 40$  K, the characteristic magnetization dynamic parameters for the systems have been extracted on the basis of an Arrhenius model, i.e.,  $\tau = \tau_0 \exp(\Delta E/k_B T)$ . The estimated energy barrier in the thermally activated process,  $\Delta E = 614(11)$  K, is smaller than that found for the crystalline phase of TbPc<sub>2</sub> (965 K)<sup>[35]</sup> but in line with the value observed in similar conditions for amorphous unfunctionalized TbPc<sub>2</sub> systems,<sup>[32]</sup> in agreement with the amorphous character of Tb[Pc<sub>2</sub>(PO<sub>3</sub>Et<sub>2</sub>)<sub>2</sub>]<sub>2</sub> sample. The extracted pre-exponential factor is  $\tau_0 = 17(4) \times 10^{-11}$  s. Below 40 K the relaxation becomes temperature independent, indicating the onset of a tunnel mechanism of inversion

Q3



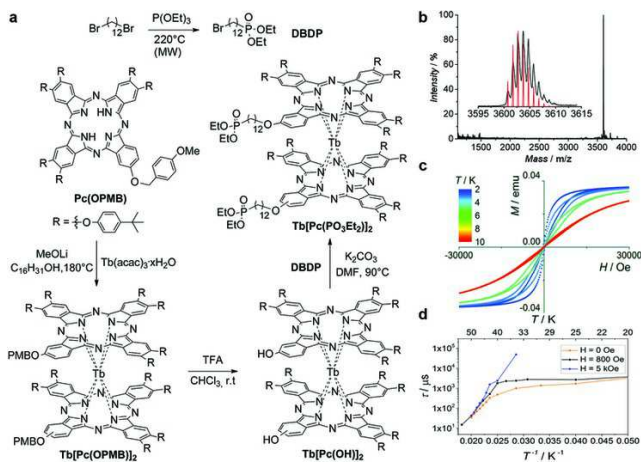


**Figure 1.** a) Synthesis of  $\text{Tb}[\text{Pc}(\text{PO}_3\text{Et}_2)]_2$ . b) High-resolution MALDI-TOF spectrum of  $\text{Tb}[\text{Pc}(\text{PO}_3\text{Et}_2)]_2$ , with experimental (black line) versus theoretical (red line) isotopic distribution in the inset. c) Magnetization versus field measurements of  $\text{Tb}[\text{Pc}(\text{PO}_3\text{Et}_2)]_2$  performed in the temperature range between 2 and 10 K (color scale in the inset) and scanning the field between 30 and  $-30$  kOe at  $50$  Oe  $\text{s}^{-1}$ . d) Relaxations times of  $\text{Tb}[\text{Pc}(\text{PO}_3\text{Et}_2)]_2$  against inverse temperature (for the temperature range 20–55 K) at three different static magnetic fields: 0 Oe, 800 Oe, and 5 kOe.

Q4

of magnetization, with a significant increase of the width of the distribution of the relaxation times (see the Supporting Information). The application of a static field (Figures S5 and S6, Supporting Information) leaves unaltered the high temperature behavior as shown in Figure 1d, but significantly affects the magnetic relaxation below 40 K, suppressing the tunneling mechanism with  $\tau$  exceeding the accessible timescale of the AC susceptometry. A narrower distribution of  $\tau$  is observed in static field in analogy to what previously found for other functionalized and unfunctionalized  $\text{TbPc}_2$  complexes.<sup>[35, 36]</sup> This can be explained with the fact that, when tunneling is not suppressed by the external field, the distortions from idealized  $\text{D}_{4d}$  strongly affect the tunneling efficiency.

## 2.2. Chemisorption of the Tb Double-Decker on LSMO

The deposition of  $\text{Tb}[\text{Pc}(\text{PO}_3\text{Et}_2)]_2$  on LSMO has been achieved by implementing the same procedure previously described for the self-assembly of nitronyl nitroxide radicals functionalized with the diethyl-phosphonate group.<sup>[22]</sup> In parallel, also the deposition of a  $\omega$ -iodo alkyl-phosphonate, the diethyl(11-iodoundecyl)phosphonate, has been performed to obtain a reference diamagnetic layer to be used in the following steps (see the Supporting Information for details). Chemisorption of these molecular layers (see the Experimental Section for details) has been verified by X-ray photoelectron spectroscopy (XPS). Focusing on the grafting of  $\text{Tb}[\text{Pc}(\text{PO}_3\text{Et}_2)]_2$ , this spectroscopic characterization (see Figure S8 in the Supporting Information) confirms the intactness of the molecular layer. Due to the presence of interfering signals, only the  $\text{Tb}3d_{3/2}$  (at 1277.7 eV and a shake-up at 1282.7 eV)<sup>[37, 38]</sup> and N1s signals have been used for this analysis. The N/Tb ratio is  $16.7 \pm 1.0$ , perfectly in line with the expected value (16); additionally, the N1s peak fitting

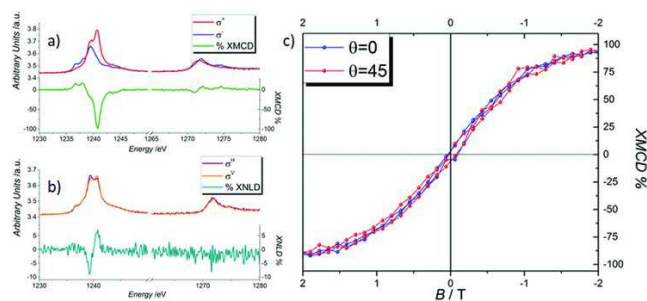


**Figure 2.** a) XMCD measurements at  $2.2 \pm 0.2$  K under a 30 kOe magnetic (green line is obtained from the difference of the left ( $\sigma^+$ , red line) and right ( $\sigma^-$ , blue line) polarized light and b) XNLD measurements for  $\text{TbPc}_2$ @LSMO performed at  $2.2 \pm 0.2$  K under a 30 kOe magnetic field to enhance detection sensitivity. XNLD (dark green line) is obtained from the difference of the horizontally ( $\sigma^H$ , purple line) and vertically ( $\sigma^V$ , orange line) polarized light. c) Field dependence of the XMCD signal measured at the maximum of the dichroic signal at the  $M_5$  edge for  $\text{TbPc}_2$ @LSMO. The curves are reported at two angles,  $\theta$ , between the magnetic field and the surface normal ( $\theta = 0^\circ$  and  $\theta = 45^\circ$ ).

reveals two components at 398.5 eV and at 400.2 eV. The first peak is directly attributable to a nitrogen in the bulk  $\text{TbPc}_2$ <sup>[39]</sup> while the other one at higher energy (400.2 eV) suggests that part of the chemisorbed molecules are influenced by the substrate, in analogy to what observed for similar complexes chemisorbed on  $\text{Si}$ .<sup>[21]</sup>

To characterize the magnetic behavior of the hybrid system an X-ray absorption spectroscopy (XAS)-based study using circularly polarized light has been performed to extract the XMCD contribution and its magnetic field dependence at low temperature ( $2.2 \pm 0.2$  K) for both substrate and molecular layer. Absorption and dichroic spectra measured at the  $L_{2,3}$  edges of Mn (Figure S9, Supporting Information) exhibit the standard LSMO features in perfect agreement with previous reports.<sup>[40, 41]</sup> Analogously the XAS and XMCD investigations at Tb  $M_{4,5}$  edges, reported in Figure 2, show the expected  $\text{TbPc}_2$  spectral features<sup>[31]</sup> and the “edge jump” analysis<sup>[42]</sup> of the derived isotropic spectrum confirms the formation of a deposit of the order of 0.8 monolayer if compared to a monolayer deposit of  $\text{TbPc}_2$  sublimated on LSMO.<sup>[43]</sup> The magnetization curves extracted for the  $L_3$  edge of Mn (Figure S9, Supporting Information) show the typical angular dependence of LSMO thin films with in-plane magnetic anisotropy.

On the other hand, the magnetization curves obtained at the Tb  $M_5$  edge (Figure 2c) do not follow the behavior of the LSMO substrate excluding the presence of a strong magnetic coupling between the molecular layer and the ferromagnetic substrate in contrast to what found in other hybrid  $\text{TbPc}_2$ -based assemblies.<sup>[44–46]</sup> It has to be noticed that the presence of the small hysteresis confirms the persistence of the SMM behavior even if, independently to the orientation of the sample, it is characterized by a much narrower opening than the one recorded by either conventional magnetometry (Figure 1c) or XMCD (Figure S10, Supporting Information) in the bulk phase. Analogies of this behavior with earlier reports<sup>[31, 32, 43]</sup> are evident and can be partially justified by distortion of the molecular structure induced by the chemisorption on the LSMO substrate.

Linearly polarized light was also used in order to get information about the orientation of the molecules with respect to the surface. The derived X-ray natural linear dichroism (XNLD) spectrum measured at  $\theta = 45^\circ$  (Figure 2b) shows a small dichroic contribution indicative of a slightly preferential molecular orientation on the surface with the phthalocyanine rings parallel to the plane of the LSMO surface. We notice the opposite trend with respect to unfunctionalized  $\text{TbPc}_2$  molecules deposited by sublimation on LSMO that tend to assemble with a standing configuration.<sup>[43]</sup>

### 2.3. Device Preparation and Characterization

The effects induced by the SMM layer on the spin injection process have been investigated by the direct comparison of two specially designed organic spin valve devices (OSV) differing only by the presence or the absence of the  $\text{TbPc}_2$ , while keeping similar all the other parameters. Vertical cross-bar geometry has been employed with LSMO as bottom and Co as top electrodes, 40 nm of tris(8-hydroxyquinoline) gallium(III) ( $\text{Gaq}_3$ ) as charge/spin transport layer, and an aluminum oxide buffer layer between the  $\text{Gaq}_3$  and Co.<sup>[47,48]</sup> The two ferromagnetic electrodes are characterized by different coercive field values allowing the achievement of parallel and antiparallel relative orientations of their magnetic moments and enabling the spin valve functionality.<sup>[49]</sup> In both sets, the LSMO electrode has been functionalized by chemisorbing a single layer of alkyl-phosphonate molecules. The first set contained the  $\omega$ -iodo alkyl-phosphonate to chemically tailor the bottom injecting interface, while the second set has been additionally characterized by the presence of SMM centers (see Figure 1a).

Figure 3 reports the  $I$ - $V$  characteristics measured at different temperatures in the range 3–300 K for the devices bearing respectively the  $\omega$ -iodo alkyl-phosphonate and  $\text{Tb}[\text{Pc}(\text{PO}_3\text{Et}_2)]_2$ . The two different functionalizations sketched in Figure 3 do not induce qualitative modifications: both sets show typical trends for this geometry and electrodes<sup>[7,50]</sup> and can be tentatively described by transport via both the LUMO (or HOMO) level<sup>[51]</sup> or the impurity band.<sup>[52]</sup> The observed increase in the resistivity values when  $\text{Tb}[\text{Pc}(\text{PO}_3\text{Et}_2)]_2$  is present could be reasonably attributed to an increased thickness of the chemisorbed layer or to a different transport efficiency of the embedded system.

The magnetoresistance (MR) detected for the two sets of devices for the 5–200 K temperature interval is presented in Figure 4. The in-plane magnetic field was swept from  $-1$  T to  $+1$  T and vice versa while measuring the device resistance in a four-point probes configuration at a fixed  $0.5 \mu\text{A}$  applied current.

Both types of devices feature inverse spin-valve effect, i.e., the lower resistance corresponds to antiparallel Co and LSMO magnetizations (see the cartoons in Figure 4). This behavior is typical for OSV devices based on LSMO-quinolines-Co systems and was confirmed for a number of spin valve devices.<sup>[7,8,22,50]</sup> It is generally accepted that the fundamental contribution to this inversion comes from the interfacial hybridization between one or both magnetic electrodes and the organic molecules (the so called spinterface effect).<sup>[22,53]</sup> We thus note that the performed functionalization does not induce qualitative changes to this generally established picture.

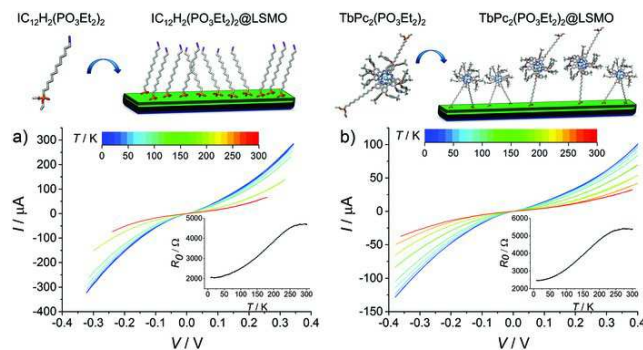


Figure 3.  $I$ - $V$  characteristics for OSV functionalized a) with  $\omega$ -iodo alkyl-phosphonate and b) with  $\text{Tb}[\text{Pc}(\text{PO}_3\text{Et}_2)]_2$  at different temperatures (color scale in the inset). In the insets, the values of resistance are also reported (measured at  $I = 0.5 \mu\text{A}$  and with no magnetic field present) as function of temperature in the range 3–300 K. On top of both  $I$ - $V$  curves, the chemisorption on LSMO of the two molecules is depicted.

Q5

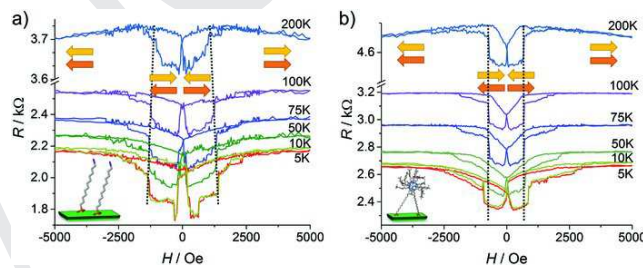
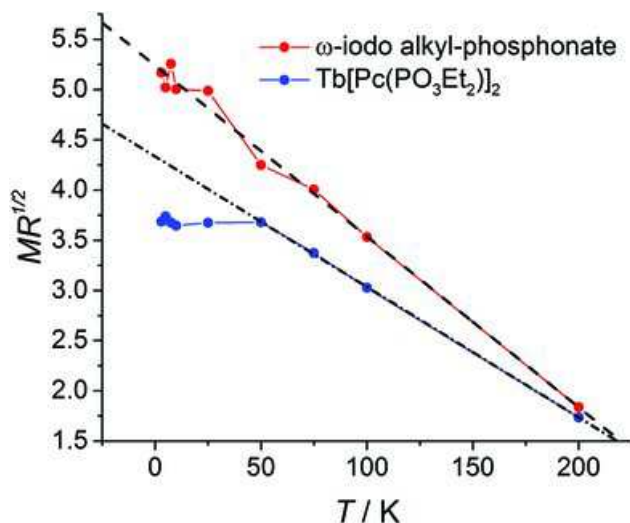


Figure 4. Inverse spin-valve effect measured sourcing a constant current  $I = 0.5 \mu\text{A}$  for a)  $\omega$ -iodo alkyl-phosphonate and b)  $\text{Tb}[\text{Pc}(\text{PO}_3\text{Et}_2)]_2$ -based OSV in the temperature range 5–200 K: the high and low resistance states correspond to parallel and antiparallel configurations, respectively (see the cartoons). Dotted lines are guides to the eyes to follow the temperature dependence of high switching fields.

We also observe a fine structure for the antiparallel resistive section detected at low temperatures for the  $\omega$ -iodo alkyl-phosphonate set of measurements. Such features are quite typical for OSV and even inorganic devices and are basically attributed to local imperfections of electrodes, an effect which is beyond the scope of this paper.

In order to unveil the contribution of the SMM layer to the interfacial effects a quantitative analysis of data has to be employed. The first statistically relevant difference between the two sets is noticeable for the switching fields. The low switching fields in both types of devices closely correspond to the coercive fields of Co electrodes (see Figure S11 in the Supporting Information). Conversely, the high switching fields significantly exceed those of the manganite electrodes (see Figure S12 in the Supporting Information), and can be tentatively attributed to the hybrid LSMO- $\text{PO}_3\text{Et}_2$  bilayers, similarly to previously reported chemisorbed interfaces,<sup>[2,54]</sup> resulting as the most sensitive region of the field scan to the alterations we operated. In fact these switching fields feature a remarkably different behavior: when the LSMO is functionalized with the alkyl-phosphonate layer, the external switching fields increase by decreasing the temperature as expected for ferromagnetic thin films (see Figure 4a).<sup>[55]</sup> On the other hand, when the  $\text{TbPc}_2$  molecule is integrated at the in-





**Figure 5.** Square root of the MR as function of temperature for representative devices from the two sets. Red circles represent the OSV with LSMO functionalized with the  $\omega$ -iodo alkyl-phosphonate while blue circle the ones functionalized  $\text{Tb}[\text{Pc}(\text{PO}_3\text{Et}_2)_2$ . The black lines are guides to the eye.

terface, the standard magnetic behavior is no longer detected for LSMO-based electrode: the switching fields surprisingly become temperature independent above 50 K (see Figure 4b).

The same temperature of about 50 K separates two different regimes also for the strength of magnetoresistance as function of temperature. **Figure 5a** shows the square root of the MR versus  $T$ . The  $\text{MR}^{1/2}(T)$  plot is linear in standard LSMO-based spin valves (without additional functionalization), whose temperature dependence is mainly governed by LSMO surface spin polarization.<sup>[22]</sup> While the  $\omega$ -iodo alkyl-phosphonate set generally obeys this standard temperature dependence (red dots in Figure 5), a clear deviation from linear behavior for  $T < 50$  K is visible for samples with LSMO electrodes functionalized with the  $\text{TbPc}_2$  (blue dots).

A pictorial comprehensive representation of the OSV behavior is proposed in **Figure 6** as an useful approach to describe the temperature dependence of the magneto-transport behavior of the devices. Here, we show the maps of the absolute value of normalized differences between the MR measurements obtained sweeping the magnetic field from negative to positive values and those obtained in the way back, for two representative devices from the two batches. The device with the monolayer of  $\omega$ -iodo alkyl-phosphonate is characterized by a temperature dependent hysteresis (with coercive fields that vary linearly from 1400 Oe at 3 K to 1000 Oe at 250 K). On the opposite,  $\text{TbPc}_2$ -based OSV, above 50 K, shows a narrower and temperature independent hysteretic behavior (coercive field is 700 Oe in almost the entire temperature range covered). This confirms the evidence from Figure 4 and represents an alternative way to figure out the information. Although in Figure 6 we cannot see each singular MR measurement, we can grasp at a glance the comprehensive trend. We reckon this as a useful pictorial device oriented representation.

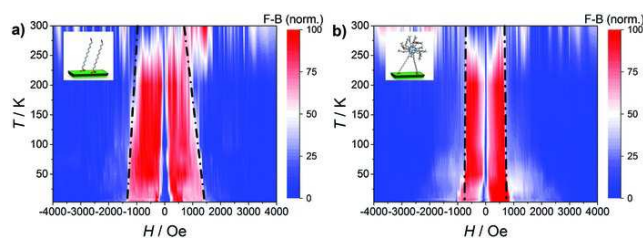


**Figure 6.** Color map of the normalized (to 100) difference between the MR measurements obtained by sweeping the magnetic field forward and backward in the range of temperature 3–300 K for the OSV functionalized a) with  $\omega$ -iodo alkyl-phosphonate and b) with  $\text{Tb}[\text{Pc}(\text{PO}_3\text{Et}_2)_2$ . The dashed and dotted black lines are only guides to the eye following the coercive fields.

### 3. Discussion

Analyzing the coercive field and magnetoresistance trends in temperature, it becomes clear that the former parameter is mainly altered above the 50 K, while the latter below this temperature. This indicates a conceptually different contribution of  $\text{Tb}$  double decker on the two different parameters. To understand these effects it is necessary to analyze the process of the spin injection that governs the magnetoresistance and related measurable parameters and, on the other hand, to consider the magnetic properties of the added molecule. Starting from the MR we can limit our analysis to the case when LSMO injects carriers and spins; inverting the current, i.e., collecting spins with LSMO, does not change the physical picture. The charge-spin injecting interface represents a complex system, where the injecting surface is composed of the last metallic layer strongly hybridized with the first molecular layer; this is followed by partly modified second molecular layer and further by the 3D van der Waals molecular solid.<sup>[56]</sup> It is widely agreed that the injection of carriers proceeds via a two-step process: the tunneling event from the injecting surface into the first nonhybridized layer and the subsequent diffusion of carriers (polarons) into the bulk of molecular solid.<sup>[57]</sup> There the transport proceeds via hopping processes, where the carriers “jump back and forth” gradually moving the polaron to the neighboring site.<sup>[58]</sup> In our case the injecting surface is represented by the LSMO-alkylphosphonate bilayer, while the first nonhybridized molecular layer is the  $\text{TbPc}_2$ , with its strong paramagnetic behavior at these temperatures. The last injecting step is then represented by the diffusion from the double decker to the bulk of  $\text{GaQ}_3$ . It is clear that, as far as the spin transfer is concerned, the injection process can be strongly affected by the paramagnetic scattering. The decrease of the MR with respect to the expected temperature trend may be explained by an additional spin scattering induced by  $\text{TbPc}_2$  molecules. This scattering is supposed to proceed via a partial transfer of the magnetic momentum from incoming charges and localized impurities, like in doped inorganic semiconductors.<sup>[59]</sup> The scattering is thus expected to depend on the interaction with these magnetic centers and their magnetic dynamics. On the basis of earlier descriptions of the  $\text{TbPc}_2$  electronic structure<sup>[60]</sup> we can exclude a direct involvement of the localized 4f orbitals of  $\text{Tb}^{3+}$  ion in the transport process. More probably charge transfer can occur here through the singly occupied molecular orbital delocalized on the phthalocyaninato ligands. Carriers can feel the mag-

netic moment of the SMM through space (dipolar interaction) or through a weak, bond-mediated, exchange interaction.<sup>[61,62]</sup> We remind that the TbPc<sub>2</sub> system has its own intrinsic dynamics defined by its characteristic relaxation time  $\tau$  introduced in paragraph 2.1. At 50 K the relaxation time value is, also in presence of magnetic fields of the order of those experienced in the device, of the order of 10  $\mu$ s (see Figure 1d) and this parameter is extraordinary close to the carrier diffusion time ( $\tau_d$ ) in Gaq<sub>3</sub>. Indeed the mobility in the quinolines is notably in the interval of  $10^{-4}$ – $10^{-5}$  cm<sup>2</sup> V<sup>-1</sup> s<sup>-1</sup> with corresponding diffusion times between 1 and 10  $\mu$ s respectively, as evaluated from the Einstein equation.<sup>[63]</sup> From the model of charge injection described above, it is clear that the diffusion inside Gaq<sub>3</sub> represents the “escape channel” (or the “arrival gate,” according to the polarity) for carriers localized in the frontier orbitals of TbPc<sub>2</sub>. This diffusion process defines the time along which the injected spins (or the collected ones) are exposed to the magnetic scattering interaction

The sizeable reduction of the magnetoresistance with respect to the case without the SMM monolayer (Figure 5a) can thus be attributed to an additional scattering. Although a description of the microscopic mechanisms of such scattering is still lacking, some possible general trends can be figured out from the involved time scales and their temperature dependences by considering two limit cases, namely  $\tau_d \ll \tau$  and  $\tau_d \gg \tau$ . In the first case, the magnetic dynamics of the TbPc<sub>2</sub> molecule is slower than the charge diffusion process through the Gaq<sub>3</sub>: this means that its magnetic moment may be considered fixed with respect to the moving carrier. The latter will thus experience, each time it interacts during its diffusive walk with a TbPc<sub>2</sub> molecule, the molecular magnetic moment as an additional local static field, the precession around which will partially modify its spin, inducing an additional decrease of magnetoresistance (Figure 5a). In the opposite case,  $\tau_d \gg \tau$ , the dynamics of TbPc<sub>2</sub> is faster than the charge carrier diffusion time and the spin scattering channel cannot be established: the MR is again fully governed by the manganite spin polarization. This model allows to describe the MR(*T*) behavior observed in the OSVs studied: when  $T > 50$  K we are in the  $\tau_d \gg \tau$  case (see Figure 1d) and MR(*T*) follows the surface magnetization of the LSMO electrode being linearized in the MR<sup>1/2</sup> versus *T* plot.<sup>[50]</sup> Once temperature is lower than 50 K the system enters in the  $\tau_d \ll \tau$  regime: a new scattering channel is present which constitutes a bottleneck for spin polarized currents leading to the plateau observed in MR(*T*) curves of OSV comprising TbPc<sub>2</sub> molecules. Devices functionalized with  $\omega$ -iodo alkyl-phosphonate are instead not affected by this additional magnetic scattering channel and their MR(*T*) is indeed determined only by manganite spin polarization.

Considering the coercive fields and their trend with temperature, we note that this parameter is strongly modified, in contrast to MR, above 50 K, that is in the pure paramagnetic regime of TbPc<sub>2</sub>. The coercive field  $H_C$  represents the applied field value for which half of the magnetic volume has switched its magnetization direction and is strongly related to the dynamics of the domain wall motion.<sup>[64]</sup> In a magnetoresistance experiment the sensing probe is the spin of the charge carriers, i.e., these magnetic processes are seen from the carriers' perspective. The coercive fields ascribed to the LSMO interface are higher than those

measured directly on manganite films. This is a typical scenario in OSVs and can be ascribed to the modification of the surface magnetism of LSMO (or other electrode) via the hybridization with grafting molecules of the SAM.<sup>[54]</sup> It is reasonable to assume that a layer of fast relaxing TbPc<sub>2</sub> magnetic moments in contact with this hybridized interfacial layer, may modify the magnetic dynamics of the latter. We can suppose that considering separately the spinterface, i.e., the bilayer formed by the surface of LSMO and the alkyl-phosphonate, is not sufficient to describe the magnetic reversal process because of the additional dipolar interaction of this bilayer with the magnetic molecules. Nevertheless, to the best of our knowledge there are no available models able to treat these effects. The presence of a strong magnetic layer in the vicinity of the spin injecting surface may represent a powerful tool for the investigation of the magnetic dynamics and other key magnetic parameters and we believe that understanding this from both experimental and theoretical point of view is crucially important.

## 4. Conclusions

A new derivative of TbPc<sub>2</sub> engineered for the LSMO functionalization has been produced and used to create an additional spinterface in a vertical organic spin valve. The behavior of this hybrid spin valve has been compared with that of a similar device fabricated by the chemisorption of a diamagnetic alkyl-phosphonate system in order to disentangle the role of the chemisorbing agent from the additional effects due to the introduction of an almost decoupled SMM which behavior has been preliminarily evaluated by XAS-based techniques.

The crafted spinterface plays an active role establishing an additional spin-scattering layer able to control directly the MR strength. This regime is active below a threshold temperature that can be correlated to the characteristic timescale of the dynamics of the SMMs. Above this critical temperature an unusual effect of freezing the coercive fields of the vicinal to SMM magnetic electrode was detected. The observed results open novel perspectives on the use of these molecular layers with a controlled magnetism for a functional tailoring of the spinterface, although a deeper understanding of the interaction between the carriers' spins and single molecule magnets is strongly required.

## 5. Experimental Section

*Synthesis Details:* Reagents used as starting materials and commercial solvents were used as received without further purification. Unless stated otherwise, reactions were conducted in flame-dried glassware under an atmosphere of argon using anhydrous solvents (either freshly distilled or passed through activated alumina columns). Silica column chromatography was performed using silica gel 60 (Fluka 230–400 mesh or Merck 70–230 mesh). NMR spectra were obtained using a Bruker AVANCE 300 (300 MHz) and a Bruker AVANCE 400 (400 MHz) spectrometer at 25 °C. All chemical shifts ( $\delta$ ) in <sup>1</sup>H NMR and <sup>31</sup>P NMR were reported in ppm relative respectively to the proton resonances resulting from incomplete deuteration of the NMR solvents and

to external 85%  $\text{H}_3\text{PO}_4$  at 0.00 ppm. High-resolution MALDI-TOF mass spectrometry was performed on an AB SCIEX MALDI TOF-TOF 4800 Plus (matrix: *a*-cyano-4- hydroxycinnamic acid). UV-vis spectra were collected using a Thermo Scientific Evolution 260 Bio spectrophotometer equipped with a Peltier water-cooled cell changer device, using matched quartz cells of 1 cm path length. Phthalocyanine Pc(OPMB) was prepared according to modified published procedures.<sup>[30]</sup>

Diethyl 12-bromododecylphosphonate (DBDP). A mixture of 1,12-dibromododecane (2.0 g, 6.1 mmol) and triethylphosphite (0.35 mL, 2.0 mmol) was stirred at 220 °C under microwave irradiation for 5 min. The resulting solution was dried under vacuum and the residue was purified by flash column chromatography (ethyl acetate/hexane 7:3) to give PBDP (0.7 g, 1.8 mmol, 90%) as a colorless oil.  $^1\text{H}$  NMR (400 MHz,  $\text{CDCl}_3$ ,  $\delta$ ): 4.08 (q, 4H,  $J = 6.1$  Hz,  $\text{POCH}_2$ ), 3.39 (t, 2H,  $J = 6.7$  Hz,  $\text{BrCH}_2$ ), 1.83 (q, 2H,  $J = 6.9$  Hz,  $\text{CH}_2$ ), 1.70 (m, 2H,  $\text{CH}_2\text{P}=\text{O}$ ), 1.57 (m, 2H,  $\text{CH}_2$ ), 1.42–1.25 (m, 22H,  $\text{CH}_2$  and  $\text{CH}_3$ );  $^{31}\text{P}\{^1\text{H}\}$ NMR (162 MHz,  $\text{CDCl}_3$ ,  $\delta$ ): 32.7 (s,  $\text{P}=\text{O}$ ); ESI-MS  $m/z$ : 385.2  $[\text{M}+\text{H}]^+$ , 407.4  $[\text{M}+\text{Na}]^+$ , 425.1  $[\text{M}+\text{K}]^+$ .

$\text{Tb}[\text{Pc}(\text{OPMB})]_2$ . To a dispersion of  $\text{Pc}(\text{OPMB})$  (0.127 g, 0.08 mmol) in 0.8 g of 1-exadecanol,  $[\text{Tb}(\text{acac})_3]\cdot n\text{H}_2\text{O}$  (0.018 g, 0.04 mmol), and MeOLi (0.009 g, 0.24 mmol) were added. The resulting mixture was stirred at 180 °C for 1 h. The dark-green residue was dissolved in  $\text{CHCl}_3$ , 2,3-dichloro-5,6-dicyano-*p*-benzoquinone (0.009 g, 0.04 mmol) was added, and the reaction was stirred at room temperature for 0.5 h. The solvent was removed under reduced pressure and the solid was purified by flash column chromatography ( $\text{CH}_2\text{Cl}_2$ /hexane 6:4) to give  $\text{Tb}[\text{Pc}(\text{OPMB})]_2$  as a green solid (0.046 g, 0.014 mmol, 35%). UV-vis ( $\text{CHCl}_3$ ):  $\lambda_{\text{max}} = 921, 682, 615, 479, 360, 331$ ; MALDI-TOF  $m/z$ :  $[\text{M}]^+$  calcd for  $\text{C}_{200}\text{H}_{192}\text{N}_{16}\text{O}_{16}\text{Tb}$ , 3232.396; found, 3232.352.

$\text{Tb}[\text{Pc}(\text{OH})]_2$ . Trifluoroacetic acid (3 mL) was added to a solution of  $\text{Tb}[\text{Pc}(\text{OPMB})]_2$  (0.046 g, 0.014 mmol) in 10 mL of  $\text{CH}_2\text{Cl}_2$ . The reaction mixture was stirred at room temperature for 5 h. The solvent was evaporated to yield  $\text{Tb}[\text{Pc}(\text{OH})]_2$  (0.043 g, 0.014 mmol, quant.), that was used without further purification for the next step. UV-vis ( $\text{CHCl}_3$ ):  $\lambda_{\text{max}} = 918, 681, 613, 491, 363, 330$ ; MALDI-TOF  $m/z$ :  $[\text{M}]^+$  calcd for  $\text{C}_{184}\text{H}_{176}\text{N}_{16}\text{O}_{14}\text{Tb}$ , 2992.281; found, 2992.250.

$\text{Tb}[\text{Pc}(\text{PO}_3\text{Et}_2)]_2$ . To a solution of  $\text{Tb}[\text{Pc}(\text{OH})]_2$  (0.035 g, 0.012 mmol) in 10 mL of DMF, PBDP (0.018 g, 0.048 mmol) and  $\text{K}_2\text{CO}_3$  (0.017 g, 0.12 mmol) were added. The reaction mixture was stirred overnight at 90 °C. The solvent was removed under reduced pressure and the crude was purified by flash column chromatography ( $\text{CHCl}_3$ /MeOH 98:2) to give  $\text{Tb}[\text{Pc}(\text{PO}_3\text{Et}_2)]_2$  as a green solid (0.021 g, 0.005 mmol, 48%).  $^{31}\text{P}\{^1\text{H}\}$ NMR (162 MHz,  $\text{CDCl}_3$ ,  $\delta$ ): 31.5 (s,  $\text{P}=\text{O}$ ); UV-vis ( $\text{CHCl}_3$ ):  $\lambda_{\text{max}} = 926, 680, 615, 469, 360, 330$ ; MALDI-TOF  $m/z$ :  $[\text{M}]^+$  calcd for  $\text{C}_{216}\text{H}_{242}\text{N}_{16}\text{O}_{20}\text{P}_2\text{Tb}$ , 3600.714; found, 3600.705.

**LSMO Preparation and Functionalization:** The LSMO films were grown on neodymium-gallium oxide single crystals by using the channel spark ablation technique.<sup>[64]</sup> Morphology of the electrodes has been evaluated by atomic force microscopy (see Figure S13 in the Supporting Information) prior the functionalization. These surfaces were cleaned using a protocol described elsewhere<sup>[65]</sup> and incubated at about 60 °C for 20 h in a  $2 \times 10^{-3}$  M solution of  $\text{Tb}[\text{Pc}(\text{PO}_3\text{Et}_2)]_2$  or diethyl(11-

iodoundecyl)phosphonate in a mixture 3:1 of  $\text{MeOH}/\text{CH}_2\text{Cl}_2$ . The slides were rinsed several times with pure solvents, sonicated in the solvents solution for 30 min, rinsed a second time, and dried under nitrogen flux in order to assure the removal of the molecules not directly interacting with the LSMO.

**XPS Characterization:** XPS experiments were carried out in a UHV apparatus with a base pressure in the  $10^{-10}$  mbar range. Monochromatized Al  $K\alpha$  radiation was used for XPS measurements (1486.6 eV, 100 W). The detector was a SPECS PHOIBOS 150 hemispherical analyzer mounting a 1D-DLD detector, the angle between the analyzer axis and the X-ray source was  $54.44^\circ$ . The XPS spectra were measured with a fixed pass energy of 100 eV. The binding energy scale was calibrated setting the C1s signal of the substrate at 284.5 eV. In order to minimize air exposure and atmospheric contamination, samples were mounted on sample holder under dry nitrogen environment in a portable glove bag which was then connected to the fast-entry lock system of the XPS chamber. Spectral analysis consisted in a linear background subtraction and deconvolution using a mixed Gaussian and Lorentzian line shapes for each spectral component (see the Supporting Information for further details).

**Synchrotron Characterization:** The XAS/XMCD experiments were performed on monolayer samples at the DEIMOS beamline<sup>[66]</sup> of the SOLEIL synchrotron facility. The density of photon from the X-ray beam was reduced to prevent any radiation damage. None was observed. A magnetic field up to 30 kOe was applied along the photon propagation at variable angle with the normal to the surface. The reported XAS spectra were acquired at the  $L_{2,3}$  edges of Mn and  $M_{4,5}$  edges of Tb edges under 30 kOe of magnetic field (applied parallel to the X-ray propagation vector) and using the two circular polarization (left,  $\sigma^+$  and right,  $\sigma^-$ ) at normal incidence ( $\theta = 0^\circ$ ) and rotating the sample plane  $\theta = 45^\circ$  respect to the X-ray propagation vector. XMCD is extracted as the difference  $\sigma^- - \sigma^+$ . The XNLD spectrum is the difference between vertically and horizontally polarized light absorption, both measured at  $\theta = 45^\circ$ . All the spectra were normalized following the procedures described in earlier reports.<sup>[31,67]</sup> The field dependence of the XMCD signal for both the Tb  $M_5$  edge and Mn  $L_3$  edge were recorded at  $\theta = 0^\circ$  and  $45^\circ$ .

**Spin-Valve Preparation:** The typical vertical devices were realized following the procedure described on earlier reports<sup>[9,22]</sup> using the LSMO electrodes patterned over an STO substrate and functionalized with monolayers of  $\text{Tb}[\text{Pc}(\text{PO}_3\text{Et}_2)]_2$  with alkyl-phosphonate or  $\omega$ -iodo alkyl-phosphonate. Subsequently, a 40 nm thick molecular film of  $\text{GaQ}_3$  was thermally evaporated on the functionalized LSMO surface. A cobalt electrode was then deposited together with an additional tunneling barrier constituted by a 2 nm thick  $\text{AlO}_x$  layer at the  $\text{GaQ}_3/\text{Co}$  interface in order to avoid cobalt interdiffusion inside the OSC which could led to pinholes creation between the two electrodes.<sup>[50]</sup> Using this strategy, three identical devices with an active area of 1 mm  $\times$  0.1 mm were prepared.

**Transport Measurements:** Transport measurements were performed in 4-point probes configuration using a 2601 Keithley SMU to supply current and a 2182A Keithley nanovoltmeter for voltage reading. The instrumentation was interfaced with a Quantum Design PPMS in order to perform measurements at cryogenics temperatures (down to 2.5 K) and in presence of



magnetic fields (up to 7 T). The reported characterization was carried out subsequently in each of the three devices obtained on the STO substrates for each kind of OSV revealing similar qualitative behavior.

## Supporting Information

Supporting Information is available from the Wiley Online Library or from the author.

## Acknowledgements

G.C. and L.P. contributed equally to this work. The financial support from the COST Action CA15128–MOLSPIN and the Italian MIUR through the Research through the PRIN project QC-NaMos N. 2015HYFSRT. The authors thank Dr. Gianluca Paredi of SITEIA, University of Parma, for high-resolution MALDI-TOF MS analyses and Centro Intefacoltà di Misure “G. Casnati” of the University of Parma for the use of NMR facilities. The authors acknowledge SOLEIL for provision of synchrotron radiation facilities (project 20150429) and the authors would like to thank all the staff for assistance in using DEIMOS beamline.

## Conflict of Interest

The authors declare no conflict of interest.

## Keywords

molecular magnetism, molecular spintronics, organic spin-valve, spinterface, terbium double decker

Received: June 30, 2017

Revised: July 28, 2017

Published Online: MM DD, YYYY

- [1] Y. Zhan, M. Fahlman, *J. Polym. Sci., Part B: Polym. Phys.* **2012**, *50*, 1453.
- [2] K. V. Raman, A. M. Kamerbeek, A. Mukherjee, N. Atodiresei, T. K. Sen, P. Lazić, V. Caciuc, R. Michel, D. Stalke, S. K. Mandal, S. Blügel, M. Münzenberg, J. S. Moodera, *Nature* **2013**, *493*, 509.
- [3] I. Bergenti, V. A. Dediu, M. Prezioso, A. Riminucci, *Philos. Trans. R. Soc., A* **2011**, *369*, 3054.
- [4] S. Steil, N. Großmann, M. Laux, A. Ruffing, D. Steil, M. Wiesenmayer, S. Mathias, O. L. A. Monti, M. Cinchetti, M. Aeschlimann, *Nat. Phys.* **2013**, *9*, 242.
- [5] H. Wendé, M. Bernien, J. Luo, C. Sorg, N. Ponpandian, J. Kurde, J. Miguel, M. Piantek, X. Xu, P. Eckhold, W. Kuch, K. Baberschke, P. M. Panchmatia, B. Sanyal, P. M. Oppeneer, O. Eriksson, *Nat. Mater.* **2007**, *6*, 516.
- [6] Y. Zhan, E. Holmström, R. Lizárraga, O. Eriksson, X. Liu, F. Li, E. Carlegrim, S. Stafström, M. Fahlman, *Adv. Mater.* **2010**, *22*, 1626.
- [7] Z. H. Xiong, D. Wu, Z. Valy Vardeny, J. Shi, *Nature* **2004**, *427*, 821.
- [8] V. A. Dediu, L. E. Hueso, I. Bergenti, C. Taliani, *Nat. Mater.* **2009**, *8*, 707.
- [9] M. Prezioso, A. Riminucci, I. Bergenti, P. Graziosi, D. Brunel, V. A. Dediu, *Adv. Mater.* **2011**, *23*, 1371.
- [10] C. Joachim, J. K. Gimzewski, A. Aviram, *Nature* **2000**, *408*, 541.
- [11] W. Wernsdorfer, *Int. J. Nanotechnol.* **2010**, *7*, 497.
- [12] J. Lehmann, A. Gaita-Ariño, E. Coronado, D. Loss, *J. Mater. Chem.* **2009**, *19*, 1672.
- [13] A. Ulman, *Chem. Rev.* **1996**, *96*, 1533.
- [14] D. Gatteschi, R. Sessoli, J. Villain, *Molecular Nanomagnets*, Oxford University Press, **2006**.
- [15] A. Cornia, A. C. Fabretti, M. Pacchioni, L. Zobbi, D. Bonacchi, A. Caneschi, D. Gatteschi, R. Biagi, U. Del Pennino, V. De Renzi, L. Gurevich, H. S. J. van der Zant, *Angew. Chem., Int. Ed.* **2003**, *42*, 1645.
- [16] M. Clemente-León, E. Coronado, A. Forment-Aliaga, F. M. Romero, *C. R. Chim.* **2003**, *6*, 683.
- [17] G. G. Condorelli, A. Motta, I. L. Fragala, F. Giannazzo, V. Raineri, A. Caneschi, D. Gatteschi, *Angew. Chem., Int. Ed.* **2004**, *43*, 4081.
- [18] B. Fleury, L. Catala, V. Huc, C. David, W. Zhao Zhong, P. Jegou, L. Baraton, S. Palacin, P.-A. Albouy, T. Mallah, *Chem. Commun.* **2005**, 2020.
- [19] M. Mannini, F. Pineider, P. Saintavitt, C. Danieli, E. Otero, C. Sciancalepore, A. M. Talarico, M.-A. Arrio, A. Cornia, D. Gatteschi, R. Sessoli, *Nat. Mater.* **2009**, *8*, 194.
- [20] M. Mannini, F. Pineider, C. Danieli, F. Totti, L. Sorace, P. Saintavitt, M.-A. Arrio, E. Otero, L. Joly, J. C. Cezar, A. Cornia, R. Sessoli, *Nature* **2010**, *468*, 417.
- [21] M. Mannini, F. Bertani, C. Tudisco, L. Malavolti, L. Poggini, K. Miztal, D. Menozzi, A. Motta, E. Otero, P. Ohresser, P. Saintavitt, G. G. Condorelli, E. Dalcanale, R. Sessoli, *Nat. Commun.* **2014**, *5*, 4582.
- [22] L. Poggini, G. Cucinotta, A.-M. Pradipto, M. Scarozza, P. Barone, A. Caneschi, P. Graziosi, M. Calbucci, R. Cecchini, V. A. Dediu, S. Picozzi, M. Mannini, R. Sessoli, *Adv. Mater. Interfaces* **2016**, *3*, 1500855.
- [23] M. Galbiati, C. Barraud, S. Tatay, K. Bouzehouane, C. Deranlot, E. Jacquet, A. Fert, P. Seneor, R. Mattana, F. Petroff, *Adv. Mater.* **2012**, *24*, 6429.
- [24] R. Geng, A. Roy, W. Zhao, R. C. Subedi, X. Li, J. Locklin, T. D. Nguyen, *Adv. Funct. Mater.* **2016**, *26*, 3999.
- [25] S. P. Pujari, L. Scheres, A. T. M. Marcelis, H. Zuilhof, *Angew. Chem., Int. Ed.* **2014**, *53*, 6322.
- [26] C. Queffelec, M. Petit, P. Janvier, D. A. Knight, B. Bujoli, *Chem. Rev.* **2012**, *112*, 3777.
- [27] N. W. Polaske, H.-C. Lin, A. Tang, M. Mayukh, L. E. Oquendo, J. T. Green, E. L. Ratcliff, N. R. Armstrong, S. S. Saavedra, D. V. McGrath, *Langmuir* **2011**, *27*, 14900.
- [28] V. E. Pushkarev, A. Y. Tolbin, N. E. Borisova, S. A. Trashin, L. G. Tomilova, *Eur. J. Inorg. Chem.* **2010**, *2010*, 5254.
- [29] A. Pedrini, M. Perfetti, M. Mannini, E. Dalcanale, *ACS Omega* **2017**, *2*, 517.
- [30] A. Pedrini, M. Mannini, C. Tudisco, M. Torelli, L. Poggini, A. E. Giuffrida, I. Cimatti, E. Otero, P. Ohresser, P. Saintavitt, M. Suman, G. G. Condorelli, E. Dalcanale, **2017**, unpublished.
- [31] L. Margheriti, D. Chiappe, M. Mannini, P.-E. Car, P. Saintavitt, M.-A. Arrio, F. B. de Mongeot, J. C. Cezar, F. M. Piras, A. Magnani, E. Otero, A. Caneschi, R. Sessoli, *Adv. Mater.* **2010**, *22*, 5488.
- [32] L. Malavolti, M. Mannini, P.-E. Car, G. Campo, F. Pineider, R. Sessoli, *J. Mater. Chem. C* **2013**, *1*, 2935.
- [33] S. Kyatskaya, J. R. G. Mascarós, L. Bogani, F. Hennrich, M. Kappes, W. Wernsdorfer, M. Ruben, *J. Am. Chem. Soc.* **2009**, *131*, 15143.
- [34] N. Ishikawa, M. Sugita, W. Wernsdorfer, *Angew. Chem., Int. Ed. Engl.* **2005**, *44*, 2931.

- [35] C. R. Ganivet, B. Ballesteros, G. de la Torre, J. M. Clemente-Juan, E. Coronado, T. Torres, *Chemistry* **2013**, *19*, 1457.
- [36] U. Glebe, T. Weidner, J. E. Baio, D. Schach, C. Bruhn, A. Buchholz, W. Plass, S. Walleck, T. Glaser, U. Siemeling, *ChemPlusChem* **2012**, *77*, 889.
- [37] G. Blanco, J. M. Pintado, S. Bernal, M. A. Cauqui, M. P. Corchado, A. Galtayries, J. Ghijsen, R. Sporcken, T. Eickhoff, W. Drube, *Surf. Interface Anal.* **2002**, *34*, 120.
- [38] S. S. Pitale, V. Kumar, I. M. Nagpure, O. M. Ntwaeaborwa, E. Coetsee, H. C. Swart, *J. Appl. Phys.* **2011**, *109*, 13105.
- [39] L. Lozzi, L. Ottaviano, S. Santucci, *Surf. Sci.* **2001**, *470*, 265.
- [40] S. Stadler, Y. U. Idzerda, Z. Chen, S. B. Ogale, T. Venkatesan, *Appl. Phys. Lett.* **1999**, *75*, 3384.
- [41] F. Li, Y. Zhan, T.-H. Lee, X. Liu, A. Chikamatsu, T.-F. Guo, H.-J. Lin, J. C. A. Huang, M. Fahlman, *J. Phys. Chem. C* **2011**, *115*, 16947.
- [42] P. Totaro, L. Poggini, A. Favre, M. Mannini, P. Saintavitt, A. Cornia, A. Magnani, R. Sessoli, *Langmuir* **2014**, *30*, 8645.
- [43] L. Malavolti, L. Poggini, L. Margheriti, D. Chiappe, P. Graziosi, B. Cortigiani, V. Lanzilotto, F. Buatier de Mongeot, P. Ohresser, E. Otero, F. Choueikani, P. Saintavitt, I. Bergenti, V. A. Dediu, M. Mannini, R. Sessoli, F. B. de Mongeot, *Chem. Commun.* **2013**, *49*, 11506.
- [44] A. Lodi Rizzini, C. Krull, T. Balashov, A. Mugarza, C. Nistor, F. Yakhov, V. Sessi, S. Klyatskaya, M. Ruben, S. Stepanow, P. Gambardella, *Nano Lett.* **2012**, *12*, 5703.
- [45] A. Lodi Rizzini, C. Krull, T. Balashov, J. J. Kavich, A. Mugarza, P. S. Miedema, P. K. Thakur, V. Sessi, S. Klyatskaya, M. Ruben, S. Stepanow, P. Gambardella, *Phys. Rev. Lett.* **2011**, *107*, 177205.
- [46] D. Klar, S. Klyatskaya, A. Candini, B. Krumme, K. Kummer, P. Ohresser, V. Corradini, V. de Renzi, R. Biagi, L. Joly, J.-P. Kappler, U. Del Pennino, M. Affronte, H. Wende, M. Ruben, *Beilstein J. Nanotechnol.* **2013**, *4*, 320.
- [47] Y. Q. Zhan, X. J. Liu, E. Carlegrim, F. H. Li, I. Bergenti, P. Graziosi, V. Dediu, M. Fahlman, *Appl. Phys. Lett.* **2009**, *94*.
- [48] A. A. Sidorenko, C. Pernechele, P. Lupo, M. Ghidini, M. Solzi, R. De Renzi, I. Bergenti, P. Graziosi, V. Dediu, L. Hueso, A. T. Hindmarch, *Appl. Phys. Lett.* **2010**, *97*, 162509.
- [49] I. Žutić, J. Fabian, S. Das Sarma, *Rev. Mod. Phys.* **2004**, *76*, 323.
- [50] V. Dediu, L. E. Hueso, I. Bergenti, A. Riminucci, F. Borgatti, P. Graziosi, C. Newby, F. Casoli, M. P. De Jong, C. Taliani, Y. Zhan, *Phys. Rev. B* **2008**, *78*, 115203.
- [51] J. P. Prieto-Ruiz, S. G. Miralles, H. Prima-garcía, A. Riminucci, P. Graziosi, M. Cinchetti, M. Aeschlimann, V. A. Dediu, E. Coronado, J. P. Prieto-Ruiz, S. G. Miralles, H. Prima-garcía, A. Riminucci, P. Graziosi, M. Cinchetti, M. Aeschlimann, V. A. Dediu, E. Coronado, **2016**.
- [52] Z. G. Yu, *Nat. Commun.* **2014**, *5*, 4842.
- [53] C. Barraud, P. Seneor, R. Mattana, S. Fusil, K. Bouzehouane, C. Deranlot, P. Graziosi, L. Hueso, I. Bergenti, V. Dediu, F. Petroff, A. Fert, *Nat. Phys.* **2010**, *6*, 615.
- [54] K. Bairagi, A. Bellec, V. Repain, C. Chacon, Y. Girard, Y. Garreau, J. Lagoute, S. Rousset, R. Breitwieser, Y.-C. Hu, Y. C. Chao, W. W. Pai, D. Li, A. Smogunov, C. Barreateau, *Phys. Rev. Lett.* **2015**, *114*, 247203.
- [55] J. M. D. Coey, *Magnetism and Magnetic Materials*, Cambridge University Press, **2009**.
- [56] M. Cinchetti, V. A. Dediu, L. E. Hueso, *Nat. Mater.* **2017**, *16*, 507.
- [57] V. I. Arkhipov, E. V. Emelianova, Y. H. Tak, H. Bässler, *J. Appl. Phys.* **1998**, *84*, 848.
- [58] J. T. Devreese, A. S. Alexandrov, *Rep. Prog. Phys.* **2009**, *72*, 66501.
- [59] D. Saha, L. Siddiqui, P. Bhattacharya, S. Datta, D. Basu, M. Holub, *Phys. Rev. Lett.* **2008**, *100*, 196603.
- [60] L. Vitali, S. Fabris, A. M. Conte, S. Brink, M. Ruben, S. Baroni, K. Kern, *Nano Lett.* **2008**, *8*, 3364.
- [61] R. Vincent, S. Klyatskaya, M. Ruben, W. Wernsdorfer, F. Balestro, *Nature* **2012**, *488*, 357.
- [62] I. V. Krainov, J. Klier, A. P. Dmitriev, S. Klyatskaya, M. Ruben, W. Wernsdorfer, I. V. Gornyi, *ACS Nano* **2017**, *11*, 6868.
- [63] A. Fuchs, T. Steinbrecher, M. S. Mommer, Y. Nagata, M. Elstner, C. Lennartz, F. Castet, J. Cornil, D. Beljonne, K. Seki, M. Head-Gordon, G. N. I. Clark, M. E. Johnson, T. Head-Gordon, *Phys. Chem. Chem. Phys.* **2012**, *14*, 4259.
- [64] P. Graziosi, M. Prezioso, A. Gambardella, C. Kitts, R. K. Rakshit, A. Riminucci, I. Bergenti, F. Borgatti, C. Pernechele, M. Solzi, D. Pullini, D. Busquets-Mataix, V. A. Dediu, *Thin Solid Films* **2013**, *534*, 83.
- [65] L. Poggini, S. Ninova, P. Graziosi, M. Mannini, V. Lanzilotto, B. Cortigiani, L. Malavolti, F. Borgatti, U. Bardi, F. Totti, I. Bergenti, V. A. Dediu, R. Sessoli, *J. Phys. Chem. C* **2014**, *118*, 13631.
- [66] P. Ohresser, E. Otero, F. Choueikani, K. Chen, S. Stanescu, F. Deschamps, T. Moreno, F. Polack, B. Lagarde, J.-P. Daguerre, F. Marteau, F. Scheurer, L. Joly, J.-P. Kappler, B. Muller, O. Bunau, P. Saintavitt, *Rev. Sci. Instrum.* **2014**, *85*, 13106.
- [67] M. Perfetti, M. Serri, L. Poggini, M. Mannini, D. Rovai, P. Saintavitt, S. Heutz, R. Sessoli, *Adv. Mater.* **2016**.



- Q1 APT to AU: Please provide the highest academic title (either Dr. or Prof.) for all authors, where applicable.
- Q2 APT to AU: Please provide the name of department for present address of author 'L. Poggini', if applicable.
- Q3 APT to AU: Please define the acronyms 'DCM, LUMO, HOMO, PBDP, STO, OSC, and XMCD' at their first occurrence in the text.
- Q4 APT to AU: If you have not returned the color cost confirmation form already, please email the completed form to the editorial office when you submit your proof corrections. This will confirm that you are willing to support the cost for color publication of the figures. Details about our color policies and a link to the form were included with your acceptance email. If you wish for your figures to be presented in greyscale, please email the editorial office to confirm this.
- Q5 APT to AU: Please confirm whether edits made to the sentence 'In the insets, the values of resistance...' retain the intended meaning.
- Q6 APT to AU: Please provide the publisher location in ref. (14)
- Q7 APT to AU: Please provide the correct volume number in ref. (18).
- Q8 APT to AU: Please provide the page number in ref. (47).
- Q9 APT to AU: Please provide the abbreviated journal title, volume and page number in ref. (51).
- Q10 APT to AU: Please provide the publisher location in ref. (55).
- Q11 APT to AU: Please provide the volume and page number in ref. (67).